AIAA JOURNAL
Vol. 39, No. 10, October 2001

Novel Strategy for Suppressing the Flutter Oscillations of Aircraft Wings

Benjamin D. Hall,* Dean T. Mook,† and Ali H. Nayfeh‡
Virginia Polytechnic Institute and State University, Blacksburg, Virginia 24061
and
Sergio Preidikman§
Universidad Nacional de Río Cuarto, 5800 Río Cuarto, Provincia de Córdoba, Argentina

A new strategy, based on the nonlinear phenomenon of saturation, is proposed for controlling the flutter of a wing. The concept is illustrated by means of an example with a rather flexible, high-aspect wing of the type found on such vehicles as high-altitude long-endurance aircraft and sailplanes. The wing is modeled structurally as an Euler–Bernoulli beam with coupled bending and twisting motions. A general unsteady nonlinear vortex-lattice technique is used to model the flow around the wing and provide the aerodynamic loads. The structure, the flowing air, and the controller are considered the elements of a single dynamic system, and all of the coupled equations of motion are simultaneously and interactively integrated numerically in the time domain. The results indicate that the aerodynamic nonlinearities alone can be responsible for limit-cycle oscillations and that the saturation controller can effectively suppress the flutter oscillations of the wing when the controller frequency is actively tuned.

I. Introduction

We investigate a novel strategy for suppressing the flutter of wings by means of active, nonlinear feedback control. For this investigation we combine the concepts of saturation-based control, which were recently developed by Oueini et al.[1] for externally and parametrically excited structures with state-of-the-art tools for simulating aeroelastic responses. We consider the wing structure, the flowing air, and the controller to be the elements of a single dynamic system. The nonlinear, coupled equations governing the structural dynamics, the aerodynamics, and the controller dynamics are numerically integrated in the time domain. The solution simultaneously provides the motion of the wing structure, the unsteady flowfield, as well as the commands generated by, and the response of, the controller. For a description of the numerical technique to simulate flutter, see Strganac,[2] Strganac and Mook,[3] Preidikman,[4] and Preidikman and Mook.[5] They showed that the present nonlinear aerodynamic model and a linear structural model are sufficient to predict limit-cycle oscillations.

In prior work related to the present effort, Luton and Mook[6] developed a similar numerical simulation of wing flutter, which did not use a finite element model for the wing structure, and Preidikman and Mook[7] developed a similar, two-dimensional simulation of wind-excited oscillations of long-span bridges. In both cases a linear feedback control system was added to the simulation, and a set of gains was determined to suppress the flutter well beyond the critical speed for the uncontrolled system.

In the present work we extend the nonlinear saturation-based control concept developed in Ref. 1 to include nonideal, self-excited systems and the simulation developed in Refs. 2–7 to include an active, integrated, nonlinear controller. Though the controller that we introduce here is nontraditional and modern, the concept on which it is based has a rather long history.

In 1863 William Froude[8] noted that a ship whose pitch frequency is, or nearly is, twice its roll frequency has unusual sea-keeping characteristics (see Ref. 9). It took more than 100 years to develop a thorough understanding of the roll-pitch connection. Nayfeh et al.[10] modeled the pitch and roll motions with nonlinear ordinary-differential equations that were coupled with quadratic nonlinear terms. They obtained an asymptotic approximation to the motion of such a "two-to-one" ship in head or following seas with the encounter frequency at or near the pitch frequency. The approximation exhibits the saturation phenomenon.

Saturation is the term used to describe the following behavior. Initially, when the amplitude of the excitation (wave height in the case of ships) is small, the ship pitches but does not roll. Moreover, the amplitude of the pitch motion increases linearly with the amplitude of the excitation while the roll remains unexcited, in accord with the linear theory, until a certain critical amplitude of the pitch motion is reached. At this point, the pitch motion appears to be saturated, its amplitude no longer increases when the wave height increases but remains constant, and the ship begins to roll as energy flows from the saturated pitch motion into the heretofore unexcited roll motion. The critical amplitude at which the energy transfer from pitch to roll begins depends on the damping in roll and the detuning between the natural frequencies in roll and pitch. The smaller these two quantities are, the smaller the critical amplitude is.

Although saturation was discovered in the context of ship motions, it appears in other nonlinear systems as well. Haddow et al.[11] found saturation both experimentally and theoretically while investigating modal interactions in a structure. They considered an L-shaped structure with relatively large concentrated masses near the top of the L and at the juncture of the vertical and horizontal members. By adjusting the position of the mass on the vertical member, they were able to make the first natural frequency be very nearly twice the second. The structure was excited by attaching the right end of the horizontal member to a shaker. They found that when the structure was excited near the second natural frequency the second mode quickly became saturated and energy was transferred to the first mode. Subsequently, Oh et al.[12] experimentally found the instability in ship dynamics, but most likely because of wall effects did not see saturation. Based on their observations, Haddow et al.[11] suggested the idea of exploiting the phenomenon as a passive vibration absorber. Here the idea is to make an active vibration absorber by having the structure play the roll of the pitching motion. Although

Presented as Paper 2000-0904 at the AIAA 38th Aerospace Sciences Meeting, Reno, NV, 10–13 January 2000; received 24 January 2000; revision received 25 February 2001; accepted for publication 1 May 2001.

*Graduate Research Assistant, MC 0219, Department of Engineering Science and Mechanics; currently Engineer, Pratt and Whitney, MS163-07, 400 Main Street, East Hartford, CT 06108.

†Professor, MC 0219, Department of Engineering Science and Mechanics. Associate Fellow AIAA.

‡Professor, MC 0219, Department of Engineering Science and Mechanics. Fellow AIAA.

§Professor, Faculted de Ingeniería, Ruta Nacional 36 Km 601. Member AIAA.

the motion of the structure is a combination of several free-vibration modes, they all have the same time dependence when the structure is at the point of flutter; hence, at this point the structure behaves as a single-degree-of-freedom system. The controller, which is governed by a second-order ordinary-differential equation, plays the roll of the rolling motion. The frequency of the controller is continuously adjusted so that the two-to-one ratio of the structural and controller frequencies is nearly exactly maintained at all times. As a result, the transfer of the energy absorbed from the airstream by the structure to the controller, where it can be dissipated, is greatly enhanced.

Haxton and Barr,[13] Hatwal et al.,[14] and Culvaci and Ertas[15] were unaware of the saturation phenomenon, but successfully experimented with passive control of structures via quadratically coupled vibration absorbers. Nayfeh and Zavodney[16] and Balachandran and Nayfeh[17] examined a physical system similar to that of Ref. 11. Their system was mathematically equivalent to the passive control systems examined previously, but without control. For rather large amplitudes of the excitation, they identified regions of aperiodic and chaotic motions that superseded the saturated response. Tuer et al.[18] introduced an electrical circuit as the tuned additional mode and provided active control of the free vibrations of a cantilevered beam. Oueini et al.[1] extended the work of Ref. 18 to the control of forced systems and realized practical implementations of the vibration absorber that induces the saturation phenomenon, which was proposed by Haddow et al.[11] For a thorough review of theirs and related work, see Oueini[19] (data also available on-line at http://scholar.lib.vt.edu/theses/available/etd-042399-012248/).

We employ the concepts of saturation-based control, which were developed for externally forced systems, to suppress the flutter of a wing. Unlike previous investigations, this study focuses on the control of a fluttering wing, which is an example of a nonideal,[20] self-excited system (nonideal in the sense that the aerodynamic loads and the resulting structural response are not independent and must be determined simultaneously).

The simulation tool consists of five independent modules: a model of the structure, a model of the flowfield, a model of the control system, a method for combining the models, and a time-domain numerical scheme for integrating all of the governing equations simultaneously and interactively. We balance physical accuracy with computational efficiency by using the general unsteady nonlinear three-dimensional vortex-lattice method to model the aerodynamics. Tang et al.[21] have recently demonstrated the existence of limit cycles by coupling a reduced-order vortex-lattice method with a nonlinear structural plate model, but we show, as was done in Refs. 4 and 5, that aerodynamic nonlinearities alone are sufficient to sustain limit-cycle oscillations of the wing.

II. Numerical Models

We model a wing that is typical of a sailplane or high-altitude long-endurance (HALE) aircraft. Despite the relatively slow speeds at which these vehicles travel, aeroelastic effects are a primary concern owing to the extremely flexible nature of their high-aspect-ratio wings. The structural model is linear, and the dynamics of the structure (e.g., flutter) occur around the nontrivial static equilibrium position of the wing, which is found as part of the solution. The models of the flowfield and control system are nonlinear.

A. Structural Model

The wings are modeled as cantilevered Euler–Bernoulli beams with linearly coupled bending $w(y,t)$ and twisting $\alpha(y,t)$ motions as shown in Fig. 1. The partial-differential equations governing such a beam are

$$[EI(y)w''(y,t)]'' + \mu(y)\ddot{w}(y,t) - \mu(y)r_x(y)\ddot{\alpha}(y,t) = Q_w(w,\dot{w},\ddot{w},\alpha,\dot{\alpha},\ddot{\alpha},y,t,\text{history}) \quad (1)$$

$$-[GJ(y)\alpha'(y,t)]' + I_p(y)\ddot{\alpha}(y,t) - \mu(y)r_x(y)\ddot{w}(y,t) = Q_\alpha(w,\dot{w},\ddot{w},\alpha,\dot{\alpha},\ddot{\alpha},y,t,\text{history}) \quad (2)$$

where primes denote partial derivatives with respect to the spanwise coordinate y and dots denote partial derivatives with respect to time. The physical properties are the bending stiffness $EI(y)$, the torsional rigidity $GJ(y)$, the mass per unit length $\mu(y)$, and the cross-sectional moment of inertia $I_p(y)$ of the beam; $r_x(y)$ is the separation of the inertial and elastic axes in the xy plane. $Q_w(\cdots)$ and $Q_\alpha(\cdots)$ are the generalized aerodynamic and control forces for bending and twisting, respectively.

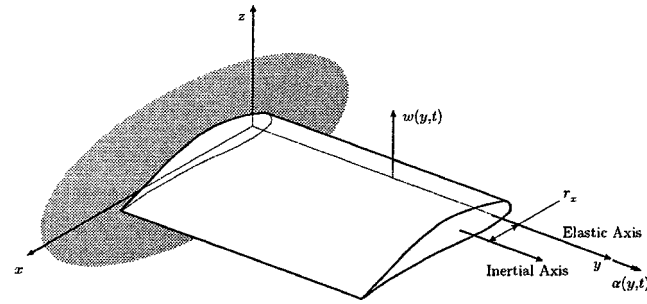

Fig. 1 Beam with an asymmetric cross section that would experience linearly, coupled bending and twisting motions.

Equations (1) and (2) are the same as those derived by Timoshenko[22] and are consistent with the reduced set derived by Rao.[23] They reduce to the classical flutter equations[24,25] when one-mode expansions are used for both the bending and torsion modes; however, one-mode expansions are not adequate for the present example.

Using the finite element method to discretize the governing equations in space, we expand the bending and torsional displacements as follows:

$$w(y,t) = \sum_{j=1}^{2N} \eta_j(y)d_j(t) \quad (3)$$

$$\alpha(y,t) = \sum_{j=1}^{N} \Theta_j(y)e_j(t) \quad (4)$$

where N is the number of elements. We use the linear finite element approximation functions for the torsional trial functions $\Theta_j(y)$ and Hermitian cubic interpolation functions for the bending trial functions $\eta_j(y)$.[26]

The spatially discretized equations are found by substituting expansions (3) and (4) into Eqs. (1) and (2), premultiplying the first equation by $\eta_i(y)$ and the second by $\Theta_i(y)$, and integrating over the length of the beam. The result is

$$\tilde{M}\ddot{\boldsymbol{x}}(t) + \tilde{K}\boldsymbol{x}(t) = \boldsymbol{F}(t) \quad (5)$$

which is a set of $3N$ coupled equations, N of which correspond to translational motion, $w(y,t)$, and have dimensions of force and the remaining $2N$ correspond to rotational motion, $\alpha(y,t)$ and $w'(y,t)$, and have dimensions of moment.

The finite element equations are uncoupled by introducing the transformation

$$\boldsymbol{x}(t) = \Phi\boldsymbol{y}(t) \quad (6)$$

where Φ is the modal matrix defined so that Eq. (5) reduces to

$$M\ddot{\boldsymbol{y}}(t) + K\boldsymbol{y}(t) = \Phi^T\boldsymbol{F}(t) \quad (7)$$

where both M and K are diagonal matrices and $\boldsymbol{y}(t)$ is the dimensionless modal vector of length $3N$. Premultiplying Eq. (7) by M^{-1}, we obtain the governing equations for the structural dynamics of the wing in terms of the finite element modes as

$$\ddot{\boldsymbol{y}}(t) + \bar{\Lambda}\boldsymbol{y}(t) = M^{-1}\Phi^T[\boldsymbol{F}_A(t) + \boldsymbol{F}_C(t)] \quad (8)$$

where $\bar{\Lambda}$ is the diagonal matrix of natural frequencies squared and we have split the force vector $\boldsymbol{F}(t)$ into aerodynamic forces $\boldsymbol{F}_A(t)$ and control forces $\boldsymbol{F}_C(t)$.

Instead of the finite element method a more direct approach is to use a Galerkin procedure on Eqs. (1) and (2). We use the finite

element method to demonstrate the versatility of this time-domain simulation; here only the modal matrix Φ, the modal masses M, and the modal frequencies $\bar{\Lambda}$ are required.

The dimensionless governing equations are

$$\ddot{\boldsymbol{y}}(\tau) + \Lambda \boldsymbol{y}(\tau) = T_c^2 M^{-1} \Phi^T [\boldsymbol{F}_A(\tau) + \boldsymbol{F}_C(\tau)] \tag{9}$$

where dots now represent derivatives with respect to the dimensionless time $\tau = t/T_c$, $\Lambda = T_c^2 \bar{\Lambda}$ is the diagonal matrix of dimensionless natural frequencies squared, and T_c is a characteristic time.

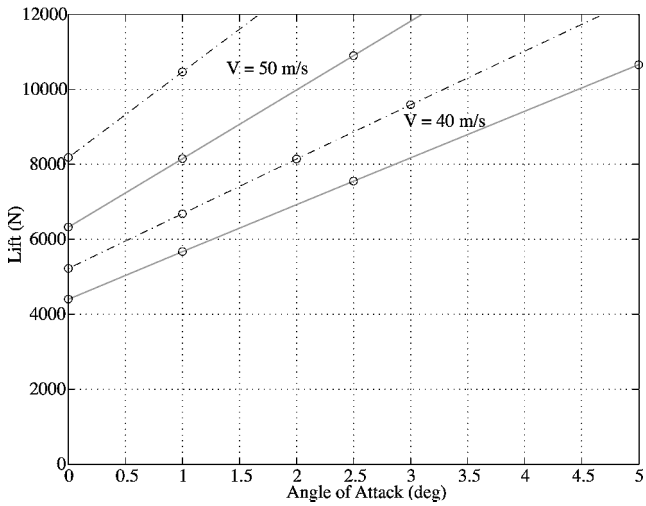

Fig. 2a Comparison of the lift forces generated by the rigid wing (– – –) and the flexible wing (——) as functions of angle of attack.

B. Aerodynamic Model

The general three-dimensional nonlinear unsteady vortex-lattice method is used to predict the aerodynamic loads. It can handle arbitrary unsteady subsonic maneuvers of wings of arbitrary planform. The method becomes unreliable when stall or vortex bursting near the wing occurs. For details, see Konstadinopoulos et al.[27] or Preidikman[4] or the works of Belotservkoskii,[28] Belotservkoskii and Lifanov,[29] or Lewis.[30] Sarpkaya[31] gives an excellent review of computational methods with vortices through the mid-1980s.

As a wing moves through air, it creates vorticity in the boundary layers that form on its surfaces and then sheds that vorticity from the wing tips and trailing edges to form the wake, or free-shear layer, behind the wing. We assume that all of the vorticity in the flowfield is located in these boundary and free-shear layers. Furthermore, we approximate these boundary and free-shear layers as infinitely thin vortex sheets. We discretize these sheets by a lattice of discrete vortex segments for computational efficiency.

The position of the bound lattice, which represents the wing, is on the camber surface and deforms with the wing during the solution. The strength of the vorticity in the free lattice, which represents the wake, is known from the solutions at earlier time steps. We use the boundary conditions to determine the strength of vorticity in the bound lattice and the position of the free lattice. These conditions are 1) on the wing lattice—no penetration condition, 2) on the wake lattice—no pressure discontinuity across the lattice, 3) interface of the wing and wake lattices—the loading vanishes, and 4) infinitely far from the wing and its wake—the disturbance created by the wing disappears. We impose the no-penetration condition on the deformed grid. This requires calculating the influence matrix at each time step.

We use the Biot–Savart law for a finite-length vortex segment to calculate the flow associated with each vortex segment of the model and the unsteady Bernoulli equation at each control point of the bound vortex lattice to calculate the loads on the wing.

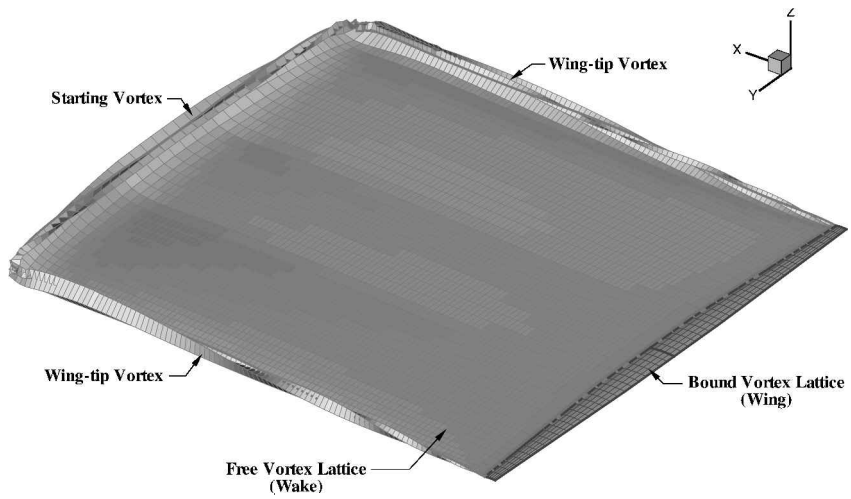

Fig. 2b Aerodynamic representation of a rigid wing and its wake.

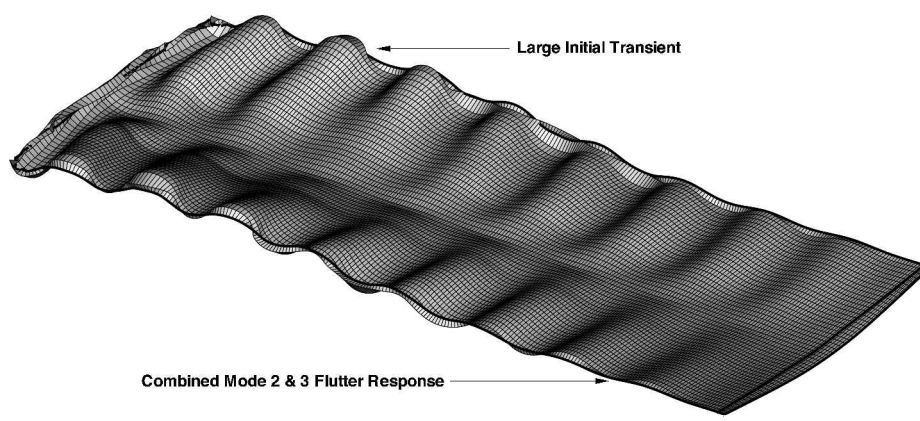

Fig. 2c Aerodynamic representation of a flexible wing responding in flutter and its wake.

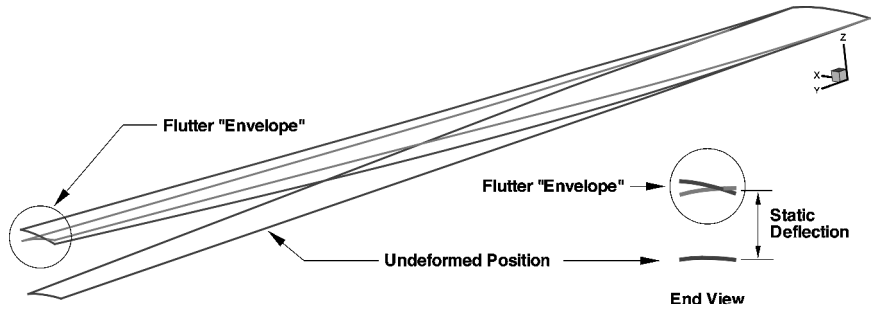

Fig. 2d Flutter response envelope of the flexible wing.

The vortex-lattice method has been widely used for aerodynamic simulations (Refs. 27–30 and 32–34) and recently for fluid-structure interaction problems (Refs. 4–7, 21, and 31), as we do here. For the present example, we model the wing as a single sheet of vorticity coincident with the wing camber surface. Figure 2 shows the lattices used for the aerodynamic simulation following an impulsive start. In Fig. 2a the steady lift for stable conditions is plotted as a function of the angle of attack for two airspeeds. The broken lines are the results for a rigid wing, and the solid lines are those for a flexible wing. Clearly, the flexibility produces a noticeable degradation in the performance. In Fig. 2b a free lattice for one of the computed wakes and the bound lattice for the rigid wing are shown. The wing tip and starting vortex systems are clearly evident. In Fig. 2c the free and bound lattices are shown for a flexible wing going into flutter. The unsteadiness is manifested in the wavy structure of the wake, in contrast with the structure of the wake in Fig. 2b. In Fig. 2d the limits of the motion of the same wing are shown. The flutter motion takes place about the unstable static equilibrium position.

The entire wake is shown for both cases, but we generally do not keep all of it. Some of the wake is necessary for predicting the flowfield around and the unsteady aerodynamic loads on the wing. The wake, which is predicted as part of the solution, is the historian of the flow. In the present simulation, we retain the wake for approximately ten chord lengths behind the wing and discard that further away.

In Fig. 3 the fast Fourier transforms (FFTs) for modes 2 and 3 are shown for several different airspeeds. The results show the merger of the frequencies associated with these two modes. The first mode essentially describes the static deflection and has a very small unsteady component at the flutter frequency. When the frequencies merge, the time-dependent coefficients in Eqs. (3) and (4) have the following form:

$$d_j(t) = D_j e^{i\omega t}, \qquad e_j(t) = E_j e^{i\omega t}$$

where ω is the flutter frequency, which depends on the amplitude of the motion, and D_j and E_j are constants. Then the expansions for the deflections, Eqs. (3) and (4), take the following form:

$$w(y,t) = \left[\sum_{j=1}^{2N} \eta_j(y)\right] e^{i\omega t}, \qquad \alpha(y,t) = \left[\sum_{j=1}^{N} \Theta_j(y)\right] e^{i\omega t}$$

The coefficients

$$\sum_{j=1}^{2N} \eta_j(y)$$

$$\sum_{j=1}^{N} \Theta_j(y)$$

are the nonlinear flutter-mode shapes.

For the calculations shown in the figures, we used the following structural parameters: $EI = 10^5$ N-m^2, $GJ = 1.5 \times 10^5$ N-m^2, $\mu = 10$ kg/m, $I_p = 15$ kg-m, and $r_x = -0.15$ m. For the aerodynamic model the wing has an aspect ratio of approximately 10, the planform is tapered, and the cross sections are those of a Wortmann FX 60-126 airfoil. The calculations were performed at an altitude of 1500 m (i.e., $\rho = 1.020$ kg/m^3), and the angle of attack was adjusted so that the static lift force was approximately equal to the weight of a typical HALE aircraft (≈10,000 N).

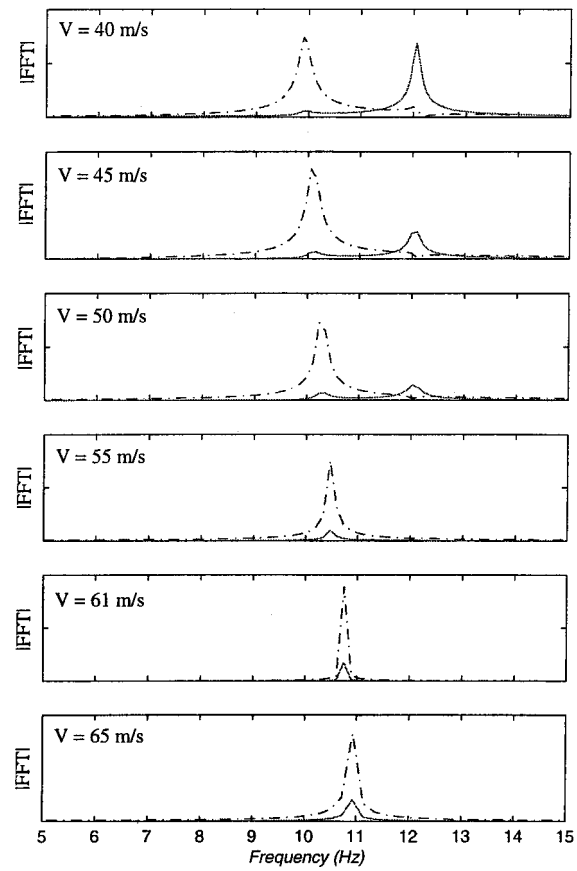

Fig. 3 Moduli of the FFTs of the mode 2 (– – –) and mode 3 (——) responses of the wing to a disturbance near the flutter boundary.

C. Controller

The level of refinement of aeroelastic control strategies has hugely increased because of the unrelenting desire to "push-the-envelope" of flight technology. Passive control strategies are still prevalent; however, active control techniques are currently receiving the most investigative efforts.

The present technique is similar to that of positive position feedback developed by Fanson and Caughey.[35] They used a tuned, second-order compensator circuit to suppress the undesirable vibrations. Instead of coupling the system to the controller linearly, they used nonlinear feedback where any appropriate quadratic coupling of position, velocity, or acceleration can be applied.[19]

The actuator applies a uniformly distributed torque along the elastic axis according to the following voltage-torque constitutive relationship:

$$\mathcal{T}(t) = K_1 \tanh\left[K_2 V(t)^2\right] \tag{10}$$

where $V(t)$ is the voltage supplied to the actuator, $\mathcal{T}$ is the output torque, and K_1 and K_2 are constants, the former representing the

actuator authority and the latter an adjustable scaling factor. The actuator torque has the nice properties of being nearly linear when K_2V^2 is small and approaching $\pm K_1$ as $K_2V^2 \to \pm\infty$.

We augment the dimensionless governing equations of motion [Eq. (9)] with the equation describing the controller dynamics:

$$\ddot{\boldsymbol{y}} + \Lambda \boldsymbol{y} = T_c^2 M^{-1} \Phi^T (\boldsymbol{F}_A + \boldsymbol{F}_C) \tag{11}$$

$$\ddot{V} + \mu_c \dot{V} + \omega_c^2 V = K_3 \dot{y}_j \dot{V} \tag{12}$$

where the voltage $V(\tau)$ is the dimensionless controller coordinate, ω_c is the controller frequency tuned to one-half the flutter frequency, μ_c is the controller damping coefficient, and $K_3 \dot{y}_j \dot{V}$ is the quadratic coupling term between the fluttering mode y_j and the controller V.

The forcing vector $\boldsymbol{F}_C(\tau)$ is the projection of the control torque onto the finite element model, which has three degrees of freedom per node and is given by

$$\boldsymbol{F}_C(\tau) = \left\{ \begin{matrix} 0 & 1 & 0 \\ \multicolumn{3}{c}{\text{(Node 1)}} \end{matrix} \middle| \cdots \middle| \begin{matrix} 0 & 1 & 0 \\ \multicolumn{3}{c}{\text{(Node N)}} \end{matrix} \right\}^T \mathcal{T}(\tau)$$

Three structural modes are used. The first is primarily the first bending mode, the second is primarily the first torsion mode, and the third is primarily the second bending mode. We write the system of equations in scalar form by defining

$$\boldsymbol{f}_a = \{f_{a1} \quad f_{a2} \quad f_{a3}\}^T = T_c^2 M^{-1} \Phi^T \boldsymbol{F}_A \tag{13}$$

where f_{aj} is the projection of the aerodynamic load on the jth structural mode; similarly, we project the nodal torques onto the modes of the structure

$$T_c^2 M^{-1} \Phi^T \boldsymbol{F}_C = \{\alpha_1 \quad \alpha_2 \quad \alpha_3\}^T \mathcal{T}(\tau) \tag{14}$$

and note that the control effort spills over onto all three modes, but the mode 2 component is much larger than the other two; that is, $\alpha_2 \gg \alpha_1$ and α_3 because the inertial coupling is weak (i.e., $r_x \ll 1$).

The scalar system of equations is

$$\ddot{y}_1 + \omega_1^2 y_1 = f_{a1} + \alpha_1 K_1 \tanh\left[K_2 V^2\right] \tag{15}$$

$$\ddot{y}_2 + \omega_2^2 y_2 = f_{a2} + \alpha_2 K_1 \tanh\left[K_2 V^2\right] \tag{16}$$

$$\ddot{y}_3 + \omega_3^2 y_3 = f_{a3} + \alpha_3 K_1 \tanh\left[K_2 V^2\right] \tag{17}$$

$$\ddot{V} + \mu_c \dot{V} + \omega_c^2 V = K_3 \dot{y}_2 \dot{V} \tag{18}$$

All modes participate in the flutter responses for the wing, but we use only the mode 2 response for the nonlinear coupling in the controller equation.

III. Combining Models

An important step in the development of this simulation is combining the structural, aerodynamic, and control models. There is no restriction on these models, and so they can be modified independently. But the simulation code must know how the deformations of the aerodynamic grid are related to the structural deformations in order to combine them correctly. Figure 4 shows crude aerodynamic and structural models overlayed. The aerodynamic mesh used in the actual simulations presented here is a 5×25 mesh, and the structural mesh has 15 elements. The aerodynamic control points are located at the centroid of the corners of each panel and are where both the no-penetration boundary condition is applied and the unsteady loads are calculated.

We must consider the projections of the structural displacements onto the aerodynamic grid and the projections of the aerodynamic loads onto the structural grid. We imagine a rigid link, perpendicular to the spanwise y coordinate, connecting each aerodynamic grid point to the structure. In general, the connecting point on the structure will not fall on a finite element node, and so the code interpolates.

The displacement of each point in the aerodynamic grid, $\boldsymbol{u}_A = \{u_x \;\; u_y \;\; u_z\}^T$, has contributions from both the displacements and rotations of the structure. For this example, we have only three degrees of freedom for the structural model $\boldsymbol{u}_S = \{\theta_1 \;\; \theta_2 \;\; u_3\}^T$. The relationship between $\boldsymbol{u}_A$ and $\boldsymbol{u}_S$ can be expressed as

$$\boldsymbol{u}_A = \begin{bmatrix} 0 & z & 0 \\ -z & 0 & 0 \\ 0 & -x & 1 \end{bmatrix} \boldsymbol{u}_s = G \boldsymbol{u}_S \tag{19}$$

where x and z are the coordinates of the aerodynamic grid point with respect to the structural connection point.

We require the virtual work done by the aerodynamic loads on the aerodynamic mesh to equal the virtual work done by the equivalent structural loads on the structural grid:

$$\delta W_A = \delta W_S$$

$$\left(\boldsymbol{F}_A^A\right)^T \delta \boldsymbol{u}_A = (\boldsymbol{F}_A)^T \delta \boldsymbol{u}_S$$

where the $\boldsymbol{F}_A^A$ are the aerodynamic loads on the aerodynamic mesh and the $\boldsymbol{F}_A$ are the equivalent aerodynamic loads projected onto the structural mesh [Eqs. (8) or (9)]. We use Eq. (19) to obtain

$$\delta \boldsymbol{u}_A = G \delta \boldsymbol{u}_S$$

and, because of the arbitrariness of $\delta \boldsymbol{u}_S$ we obtain

$$\boldsymbol{F}_A = G^T \boldsymbol{F}_A^A \tag{20}$$

IV. Time-Domain Solution

The solution is obtained by numerically integrating all of the governing equations simultaneously in the time domain. We use an adaptation of Hamming's fourth-order predictor-corrector method. At each time step we begin the calculations by convecting the wake to its new position. Then, using the current loads, velocities, and positions, we solve Eqs. (9) for the structural motions $\boldsymbol{y}(\tau)$ and Eq. (18) for the controller response $V(\tau)$. Using the latest predictions to obtain the boundary conditions for the aerodynamic model, we calculate the aerodynamic loads at the end of the time step and then re-solve (i.e., correct) for $\boldsymbol{y}(\tau)$ and $V(\tau)$. We repeat this process until there is convergence; we do not recalculate the position of the wake during this iteration. Numerical experiments have shown that other procedures in which the position of the wake is iterated do not yield noticeably different results.

V. Results

The uncontrolled (for $t < 4500$) and controlled (for $t > 4500$) responses of the structure are represented as functions of time in Fig. 5a for an airspeed of 65 m/s (about 145 mph). The results in Fig. 3 show the critical airspeed to be in the range of 50–55 m/s (about 115–120 mph), and so the response represented in Fig. 5a corresponds to an airspeed that is about 20–25% above the airspeed at the onset of flutter. These airspeeds are well within the range where an incompressible model of the flowfield can provide good results. For $t < 4500$ the results show initial transients slowly evolving into a

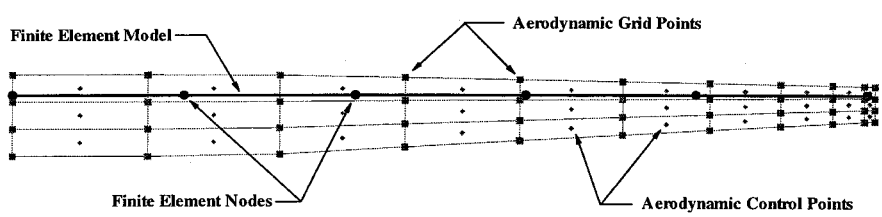

Fig. 4 Simplified picture showing the overlay of the aerodynamic and structural grids.

limit cycle. In developing the numerical simulation of the uncontrolled response, Preidikman and Mook[5] gave the wing a wide variety of initial conditions for the same airspeed and found that all of them evolved into the same limit-cycle oscillation. As the results in Fig. 3 also show, they found that the amplitude and frequency of the limit cycles that evolve increase with the airspeed. But, Preidikman and Mook also found a second critical airspeed where the system experiences a secondary subcritical Hopf bifurcation that renders the limit cycles unstable. Above this second critical airspeed, the amplitude and frequency of the limit cycles are modulated. In the present example the wing is considerably more flexible than the one considered by Preidikman and Mook, and the secondary instability occurs at an unrealistically large amplitude. All of the present results apply below the second critical airspeed.

For $t > 4500$ after the controller with a fixed frequency equal to that of the uncontrolled response at 65 m/s is activated, the results show a beating phenomenon, which is explained with the help of Fig. 5b. In this figure the frequencies of the second and third modal amplitudes are represented as functions of time. In the simulations the frequency is determined by noting the time between zero crossings of the modal amplitudes in the same direction. We see that the modes initially respond with their zero-flight-speed frequencies, but by $t = 1000$ the frequencies have essentially merged, the system is in flutter, and a limit-cycle oscillation is evolving.

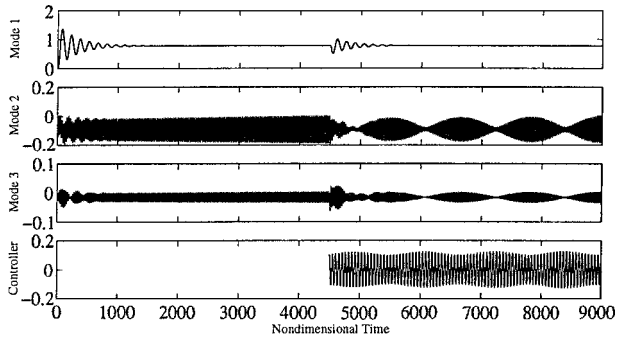

Fig. 5a Modal amplitudes and controller voltage as functions of time for the quadratically controlled system when the controller frequency is maintained constant.

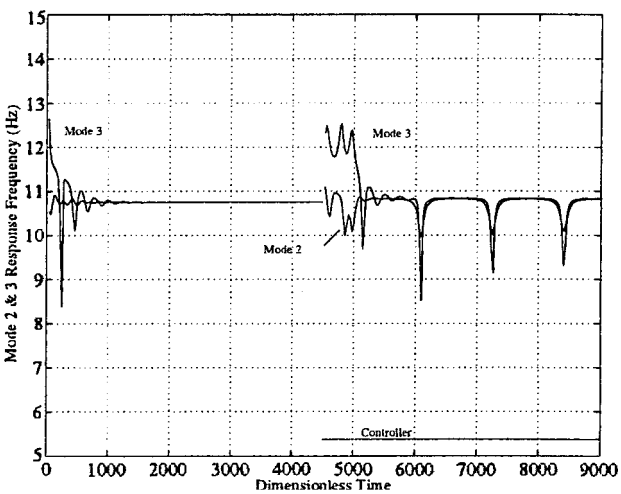

Fig. 5b Frequencies of the mode 2 and mode 3 responses as functions of time.

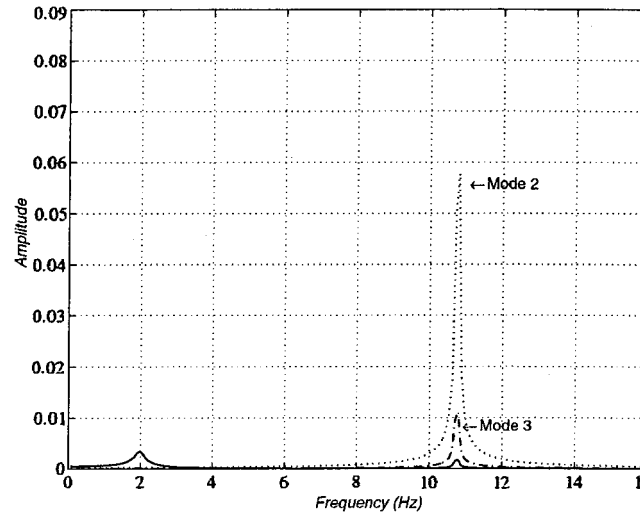

Fig. 6b FFTs of the modal responses before the control has been turned on.

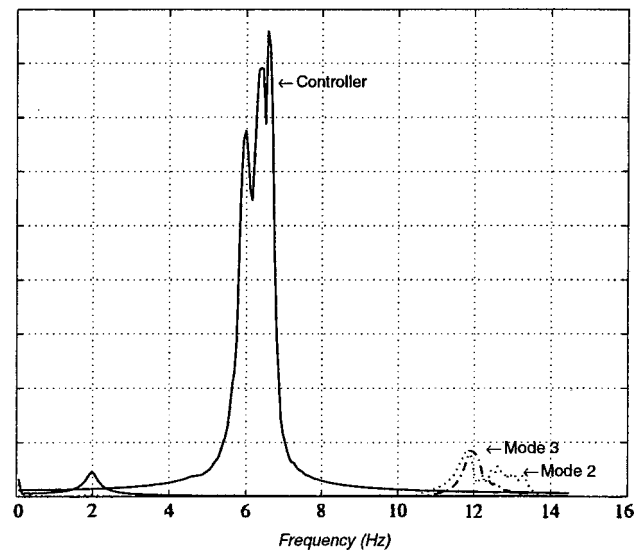

Fig. 6c FFTs of the modal and controller responses after the control has been turned on.

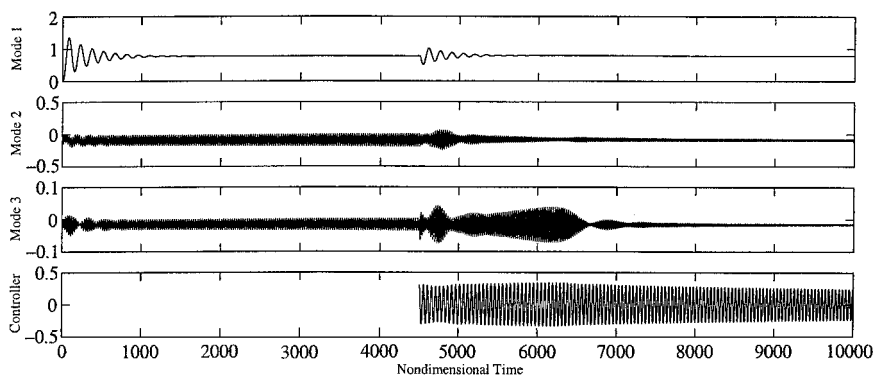

Fig. 6a Modal amplitudes and controller voltage as functions of time for the system response with quadratic velocity control implementation, before and after the controller is activated at $t = 4500$.

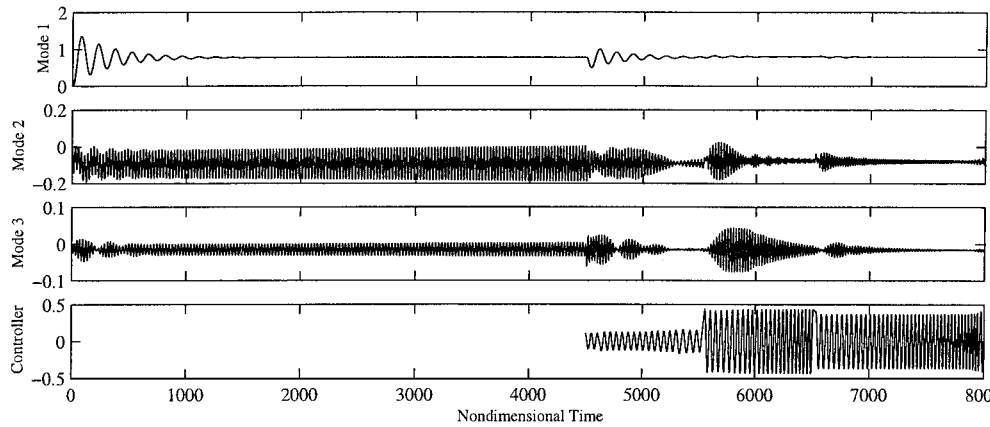

Fig. 7 Modal amplitudes and controller voltage as functions of time for the fluttering system before and after controller activation at $t = 4500$. Disturbances are input to the system at $t = 5500$ and 6500.

When the controller is suddenly activated at $t = 4500$, it introduces a strong disturbance that immediately destroys the flutter response, causing the two modal frequencies to split. But the system quickly starts to return to the old flutter attractor, and the two frequencies soon merge onto the flutter frequency for 65 m/s. The controller frequency, which is fixed in this example, is tuned to one-half of this frequency. Under the action of the controller, the amplitude of the response begins to decrease. However, when the amplitude decreases the frequency of the response also decreases detuning the control system. The detuned control system is not as effective as it was, and so the amplitude and frequency of the response begin to increase back toward the conditions that prevailed for the uncontrolled system in flutter. Then, as the amplitude and frequency increase the system retunes itself, and the controller becomes very effective again. Consequently, the amplitude and frequency stop increasing and begin to decrease again. This cycle repeats causing the beating phenomenon shown in the figure. Comparing Figs. 5a and 5b, we see that the low-frequency responses are also the low-amplitude responses.

The preceding observations lead to the conclusion that to effectively suppress the flutter we must actively tune the frequency of the controller. Oueini et al.[1] also found it necessary to adjust the frequency of the controller in their experiments on ideal, externally excited systems. In Fig. 6a the uncontrolled (for $t < 4500$) and controlled (for $t > 4500$) responses of the structure are represented for an airspeed of 65 m/s. For $t < 4500$ the results are the same as those given in Fig. 5a. Soon after the actively tuned controller is activated at $t = 4500$, some large transients develop, but they are eventually suppressed; the actively tuned, variable-frequency controller then keeps the amplitude of the motion very small. In Fig 6b the FFTs of the uncontrolled response are plotted. After some time all three modes are responding at the same frequency of nearly 11 Hz as indicated. The initial large transient in the response of the first mode produces the small peak at about 2 Hz in its FFT. In Fig. 6c the FFTs of the structural and controller responses are shown after the controller has been activated. The slowly varying frequency of both the response and the controller is responsible for the side bands and the thickening of the peaks that appear in the FFTs of both the structural and controller responses. The relatively large transients in the first mode produced by the sudden activation of the controller produce a small peak near 2 Hz in its FFT.

In Fig. 7 the response of the wing is again shown as a function of time. As before, there is no control for $t < 4500$. After the controller has been activated and the flutter suppressed, the wing is disturbed once at $t = 5500$ and once at $t = 6500$ to test the stability of the controller. In this limited test the controller quickly reduces the amplitude after each disturbance. Therefore, it appears likely that the controller is capable of suppressing the flutter and keeping it suppressed.

VI. Conclusions

We extended an existing nonlinear saturation-based control concept to nonideal, self-excited systems, and we extended earlier nonlinear unsteady aeroelastic simulations to include an active, integrated, nonlinear controller that can twist the wing. These extensions made it possible to apply this control concept to an aeroelastic problem for the first time. We showed that saturation-based control can be effectively implemented to suppress the limit-cycle oscillations of the wing, which are caused entirely by the aerodynamic nonlinearities, even when we do not explicitly know what the nonlinearities are. We found it necessary to actively adapt the controller because of the nonideal, nonlinear nature of the system, specifically the frequency–amplitude dependence.

References

[1] Oueini, S. S., Nayfeh, A. H., and Pratt, J. R., "A Nonlinear Vibration Absorber for Flexible Structures," *Nonlinear Dynamics*, Vol. 15, No. 3, 1998, pp. 259–282.

[2] Strganac, T. W., "A Numerical Model of Unsteady Subsonic Aeroelastic Behavior," Ph.D. Dissertation, Dept. of Engineering Science and Mechanics, Virginia Polytechnic Inst. and State Univ., Blacksburg, VA, Aug. 1987.

[3] Strganac, T. W., and Mook, D. T., "A Numerical Model of Unsteady Subsonic Aeroelastic Behavior," *AIAA Journal*, Vol. 28, No. 5, 1990, pp. 903–909.

[4] Preidikman, S., "Numerical Simulations of Interactions Among Aerodynamics," Ph.D. Dissertation, Dept. of Engineering Science and Mechanics, Virginia Polytechnic Inst. and State Univ., Blacksburg, VA, Oct. 1998.

[5] Preidikman, S., and Mook, D. T., "Time-Domain Simulations of Linear and Nonlinear Aeroelastic Behavior," *Journal of Vibration and Control*, Vol. 6, No. 8, 2000, pp. 1135–1175.

[6] Luton, J. A., and Mook, D. T., "Numerical Simulations of Flutter and Its Suppression by Active Control," *AIAA Journal*, Vol. 31, No. 12, 1993, pp. 2312–2319.

[7] Preidikman, S., and Mook, D. T., "A New Method for Actively Suppressing Flutter of Suspension Bridges," *Journal of Wind Engineering and Industrial Aerodynamics*, Vol. 69–71, 1997, pp. 955–974.

[8] Froude, W., "Remarks on Mr. Scott Russell's Paper on Rolling," *Transactions of the Institute of Naval Architects*, Vol. 4, 1863, pp. 232–275.

[9] Nayfeh, A. H., and Mook, D. T., *Nonlinear Oscillations*, Wiley, New York, 1979, pp. 402–417.

[10] Nayfeh, A. H., Mook, D. T., and Marshall, L. R., "Nonlinear Coupling of Pitch and Roll Modes in Ship Motions," *Journal of Hydronautics*, Vol. 7, No. 4, 1973, pp. 145–152.

[11] Haddow, A. G., Barr, A. D. S., and Mook, D. T., "Theoretical and Experimental Study of Modal Interaction in a Two-Degree-of-Freedom Structures," *Journal of Sound and Vibration*, Vol. 97, No. 3, 1984, pp. 451–473.

[12] Oh, I. G., Nayfeh, A. H., and Mook, D. T., "A Theoretical and Experimental Investigation of Indirectly Excited Roll Motion in Ships," *Philosophical Transactions of the Royal Society of London, Series A: Mathematical and Physical Sciences*, Vol. 358, 2000, pp. 1953–1991.

[13] Haxton, R. S., and Barr, A. D. S., "The Autoparametric Vibration Absorber," *Journal of Engineering for Industry*, Vol. 81, 1972, pp. 119–225.

[14] Hatwal, H., Mallik, A. K., and Ghosh, A., "Nonlinear Vibrations of a Harmonically Excited Autoparametric System," *Journal of Sound and Vibration*, Vol. 81, No. 2, 1982, pp. 153–164.

[15] Cuvalci, O., and Ertas, A., "Pendulum as Vibration Absorber for Flexible Structures: Experiments and Theory," *Journal of Vibration and Acoustics*, Vol. 118, 1996, pp. 158–166.

[16] Nayfeh, A. H., and Zavodney, L. D., "Experimental Observation of Amplitude- and Phase-Modulated Responses of Two Internally Coupled Oscillators to a Harmonic Excitation," *Journal of Applied Mechanics*, Vol. 55, Sept. 1988, pp. 706–710.

[17] Balachandran, B., and Nayfeh, A. H., "Observations of Modal Interactions in Resonantly Forced Beam-Mass Structures," *Nonlinear Dynamics*, Vol. 2, No. 2, 1991, pp. 77–117.

[18] Tuer, K. L., Golnaraghi, M. F., and Wang, D., "Development of a Generalized Active Vibration Suppression Strategy for a Cantilever Beam Using Internal Resonance," *Nonlinear Dynamics*, Vol. 5, No. 2, 1994, pp. 131–151.

[19] Oueini, S. S., "Techniques for Controlling Structural Vibrations," Ph.D. Dissertation, Dept. of Engineering Science and Mechanics, Virginia Polytechnic Inst. and State Univ., Blacksburg, VA, April 1999.

[20] Kononenko, V. O., *Vibrating Systems with a Limited Power Supply*, Iliffe, London, 1969.

[21] Tang, D., Dowell, E. H., and Hall, K. C., "Limit Cycle Oscillations of a Cantilevered Wing in Low Subsonic Flow," *AIAA Journal*, Vol. 37, No. 3, 1999, pp. 364–371.

[22] Timoshenko, S. P., Young, D. H., and Weaver, W., Jr., *Vibration Problems in Engineering*, Wiley, New York, 1974, p. 474.

[23] Rao, J. S., *Advanced Theory of Vibration*, Wiley, New York, 1992, pp. 343, 344.

[24] Fung, Y. C., *An Introduction to the Theory of Aeroelasticity*, Dover, New York, 1993.

[25] Bisplinghoff, R. L., and Ashley, H., *Principles of Aeroelasticity*, Dover, New York, 1975, p. 289.

[26] Reddy, J. N., *An Introduction to the Finite Element Method*, McGraw–Hill, New York, 1993.

[27] Konstadinopoulos, P., Thrasher, D. F., Mook, D. T., Nayfeh, A. H., and Watson, L., "Numerical Model of Unsteady Subsonic Aeroelastic Behavior," *Journal of Aircraft*, Vol. 22, No. 1, 1985, pp. 43–49.

[28] Belotserkovskii, S. M., *The Theory of Thin Wings in Subsonic Flow*, Plenum, New York, 1967.

[29] Belotserkovskii, S. M., and Lifanov, I. K., *Method of Discrete Vortices*, CRC Press, Boca Raton, FL, 1993.

[30] Lewis, R. I., *Vortex Element Methods for Fluid Dynamic Analysis of Engineering Systems*, Cambridge Univ. Press, Cambridge, MA, 1991, Chap. 8.

[31] Sarpkaya, T., "Computational Methods with Vortices—the 1988 Freemen Scholar Lecture," *Journal of Fluids Engineering*, Vol. 111, No. 75, 1989, pp. 5–52.

[32] Belotserkovskii, S. M., "Study of the Unsteady Aerodynamics of Lifting Surfaces Using the Computer," *Annual Review of Fluid Mechanics*, Vol. 9, 1977, pp. 469–494.

[33] Rom, J., Melamed, B., and Almosnino, D., "Experimental and Nonlinear Vortex Lattice Results for Various Wing-Canard Configurations," *Journal of Aircraft*, Vol. 30, 1993, pp. 207–212.

[34] Elzebda, J. M., Mook, D. T., and Nayfeh, A. H., "Numerical Simulation of Steady and Unsteady, Vorticity-Dominated Aerodynamic Interference," *Journal of Aircraft*, Vol. 31, No. 5, 1994, pp. 1031–1036.

[35] Fanson, J. L., and Caughey, T. K., "Positive Position Feedback Control for Large Space Structures," *AIAA Journal*, Vol. 28, No. 4, 1990, pp. 717–724.

E. Livne
Associate Editor